

Layer-number and strain effects on the structural and electronic properties of PtSe₂ material

Rania Amairi*

*Faculté des Sciences de Bizerte, Laboratoire de Physique des Matériaux: Structure et Propriétés,
Université de Carthage, 7021 Jarzouna, Tunisia*

Adlen Smiri†

*Mathematics for Advanced Materials Open Innovation Laboratory (MathAM-OIL),
National Institute of Advanced Industrial Science and Technology (AIST) c/o Advanced Institute for Materials Research,
Tohoku University, 2-1-1, Katahira, Aoba-ku, Sendai,
Miyagi 980-8577, Japan and Faculté des Sciences de Bizerte,
Laboratoire de Physique des Matériaux: Structure et Propriétés, Université de Carthage, 7021 Jarzouna, Tunisia*

Sihem Jaziri‡

*Faculté des Sciences de Bizerte, Laboratoire de Physique des Matériaux: Structure et Propriétés,
Université de Carthage, 7021 Jarzouna, Tunisia,
and Faculté des Sciences de Tunis, Laboratoire de Physique de la Matière Condensée and Département de Physique,
Université Tunis el Manar, Campus Universitaire, 2092 Tunis, Tunisia*

(Dated: January 9, 2024)

Abstract: Bandgap engineering of low-dimensional materials forms a robust basis for advancements in optoelectronic technologies. Platinum diselenide (PtSe₂) material has shown various electronic features when going from bulk to monolayer (ML). In this work, density functional theory (DFT) plus van der Waals (vdW) corrections have been considered to study the structural and electronic properties of different PtSe₂ systems, namely ML, bilayer (BL), trilayer (TL), fourlayer (FL) and bulk. In particular, various vdW corrections have been tested to describe the inter-layer interaction of PtSe₂ material. According to the comparison with the available experimental data, the vdW corrections vdW-DF and rVV10 gave the most accurate results. In fact, our findings show that while vdW corrections have no significant effect on the electronic structure of bulk PtSe₂, they alter that of the PtSe₂ BL, TL and FL materials. Furthermore, our calculation revealed that by decreasing the number of layers, the interlayer distance increases. In fact, a correlation between the interlayer distance and the bandgap feature was obtained. Indeed, the bandgap of PtSe₂ material increases with the increase of this distance, due to the energy shift of the Se-*p*_z dominated conduction and valence bands. Moreover, the control of the interlayer distance via vertical compressive strain led to the bandgap tuning of semiconductor PtSe₂ BL. Indeed, a semi-metal character of PtSe₂ BL can be obtained under 17% vertical strain. Our work shows a deep understanding of the correlation between the structural and electronic properties, and thus a possibility to tune the bandgap by strain means.

I. INTRODUCTION

In recent years, two-dimensional (2D) materials have attracted great interest due to their exceptional properties, which differ significantly from bulk materials [1]. The transition metal dichalcogenide (TMD) family represents an interesting and attractive group of 2D materials due to their rich electronic and optical properties [2–8]. The TMD monolayers (MLs) have the chemical formula MX₂ where M is a transition metal (Pt, Mo...) and X is a chalcogen (Se, S...). In the last decade, the TMD of group 6 of the periodic table such as 2H-MoS₂, 2H-MoSe₂ and 2H-WSe₂ have attracted the attention of the condensed matter scientific community [9, 10]. The important progress

in the control of the electronic properties of this group has stimulated the search for new two-dimensional (2D) materials. Group 10 TMD, such as PtSe₂ and PdS₂, have been discovered as promising nanostructures for applications in electronics, optoelectronics, catalysis and sensors [11–16]. Among these noble TMDs, the 1T phase PtSe₂ material attracts considerable attention due to its unique properties [17–19]. In particular, the 1T-PtSe₂ ML has high electronic mobility of 200 cm²v⁻¹s⁻¹ [20], that promotes efficient charge transport and paves the way for high-performance electronic devices such as transistors [21], photodetectors [22]. The 1T-PtSe₂ material stands out from other TMD materials due to the unique correlation between its structural and electronic properties [23–26]. Indeed, as the number of layers increases, the energy of the bandgap decreases [23–27]. This peculiarity is attributed to the interlayer coupling and screening effects [28]. The semi-metallic nature of bulk 1T-PtSe₂ has been known for a long time [29]. However, experimental studies have

* rania.amairi@fsb.ucar.tn

† smiriadlen4@gmail.com

‡ sihem.jaziri@fsb.rnu.tn

shown that $1T$ -PtSe₂ ML exhibits semiconductor behavior [30]. Additionally, a sharp decrease of the bandgap energy due to the increase of the number of layers was observed [27]. However, the exact transition between the semi-metallic and semiconductor (SM-SC) behavior of $1T$ -PtSe₂ material as a function of the layer number has not been clearly determined. Neither numerical nor experimental studies have been able to provide a clear boundary where this transition occurs. Recently, in order to solve this problem, two experimental studies were conducted [23, 24]. However, these two studies have shown two different results. In fact, *Zhang et al.* [24] showed that $1T$ -PtSe₂ material becomes a semi-metal from the fifth layer. Indeed, for a layer number that goes from one to four, the bandgap energy goes from 2.0 ± 0.1 , 1.1 ± 0.1 , 0.6 ± 0.1 and 0.2 ± 0.1 eV, respectively. However, *Li et al.* [23] proved that $1T$ -PtSe₂ material becomes a semi-metal from the third layer. In this case, the values of the bandgap energies are 1.8 eV for the PtSe₂ ML and 0.6 eV for the Bilayer (BL). Furthermore, several *ab-initio* studies have been carried out and showed discrepancies in the results [20, 26, 28, 30–32]. Therefore, to understand the effect of the layer number on the electronic properties of $1T$ -PtSe₂ material, a further insights on the origin of the SM-SC transition is needed.

For layered materials, especially TMDs, van der Waals (vdW) interactions play a crucial role, ensuring a stable connection between their layers and thereby facilitating the realisation of vdW heterostructures [33–37]. To incorporate these interactions into Density Functional Theory (DFT) calculations, various corrections have been proposed [38–42], typically grouped into two categories. The first category involves the vdW interaction by including non-local Coulomb interaction in the exchange-correlation functional, namely vdW-DF [38], vdW-DF2 [39], and rVV10 [40] functionals. The second category encompasses semi-empirical corrections, where the vdW energy is including as a correction to the total energy. For instance, DFT-D [41] and DFT-D3 [42] are empirical methods. The performance of these corrections, in the two distinct categories, varies depending on the system and properties under investigation [43–45]. Indeed, some corrections prove more effective than others for specific types of systems or properties. For example, among various vdW corrections, the DFT+rVV10 method demonstrated the best agreement with experimental results of graphite material [46]. Therefore, in order to achieve more accurate and consistent results with experimental data, these various vdW corrections should be considered for $1T$ -PtSe₂ material.

Due to their crystal structure, few-layer TMDs emerge as prime candidates for strain engineering [47–55]. Indeed, this materials have the ability to undergo significant atomic displacements without nucleating defects [51, 52]. Such materials can withstand mechanical

strain up to 30%, in contrast to silicon, which can only withstand about 1.5% [52, 56, 57]. One of the strain engineering purpose is manipulating the electronic and optical properties of these materials [49, 53–55]. In fact, the control of bandgap energy paves the way for the development of new generations of optoelectronic devices endowed with desirable properties [49, 54, 55, 58]. For instance, the application of both uniaxial and biaxial strains to MoS₂ ML allows for the modifications of its electronic and optical properties [53, 59–64], such as the bandgap energy [62], optical spectrum [65], photoluminescence [63], and mobility [64]. These modifications are crucial for its integration into various technologies, including sensors, diodes, and field-effect transistors [49, 59]. In order to broaden the applications of $1T$ -PtSe₂ material in nano-optoelectronic devices, both theoretical and experimental studies have been conducted to analyze the material response to strain, examining ML [57, 66–68], BL [69–71] systems. However, for the PtSe₂ BL under vertical compressive strain, to our knowledge while only one theoretical study was done [69], there are no existing experimental studies. In fact, the theoretical study conducted by *Li et al.* [69] have shown a reducing in the bandgap energy and SM-SC transition at large vertical compressive strain of more than 40%. This value is significantly larger than the in-plan strain that gave SM-SC transition in PtSe₂ ML [57, 72], as well as for other TMDs [73–77]. Therefore, considering different approaches to further evaluate the vertical compressive strain and understand its impact on the PtSe₂ BL is of great interest for bandgap engeneerig.

In this article, we employ DFT plus vdW corrections to investigate the layer number and strain effects on the structural and electronic properties of PtSe₂ materials. To do this, five PtSe₂ systems, namely ML, BL, trilayer (TL), fourlayer (FL) and bulk were considered. In order to reveal the effect of layer number on the structural parameters of PtSe₂ systems, We begin our work by performing a structural optimization using different vdW corrections. Then, a band structure calculations is conducted to understand the correlation between the electronic properties and the crystal structure including both layer number and crystal parameters. Finally, for a given vdW correction, the effect of a vertical compressive strain on the structural and electronic properties of PtSe₂ BL is studied.

II. COMPUTATIONAL DETAILS

Our first principle calculations are based on the Density Functional Theory (DFT) using the Quantum Espresso packages [78]. For the pseudopotential, the projected augmented wave formalism (PAW) was considered [79], and the electronic kinetic energy cutoff (E_{cut}) for the plane-wave basis was set to $544eV$. The

structural relaxation was performed using the Hellmann-Feynman Theorem [80], where the convergence threshold for forces was set to 10^{-5} u.a. To avoid inter-layer interactions, a vacuum space larger than 15\AA was used. The Brillouin zone was sampled by a fine grid of $12\times 12\times 1$ k-points for the few-layer structures and $8\times 8\times 8$ k-points for Bulk. The unit cells were visualized using the VESTA software [81]. The calculations were performed using the generalized gradient approximation (GGA) of the Perdew-Burke-Ernzerhof (PBE) functional for the treatment of the exchange-correlation interaction [82]. However, GGA+PBE fails to describe the long-range coulomb interaction such as the inter-layer vdW interaction [46, 83]. To take into account the vdW interactions, two types of vdW corrections in combination with the GGA exchange-correlation functional (GGA+PBE+vdW) were used. In particular, the first type of corrections is based on empirical approaches as defined by *Grimme*, namely DFT-D [41] and DFT-D3 [42] methods. The second type is to consider non-local functional, such as vdW-DF [38], vdW-DF2 [39], and rVV10 [40] methods. Each of these corrections has its own advantages in improving the accuracy of the calculations and getting closer results to the experimental results.

III. RESULTS AND DISCUSSION

A. Structural properties of PtSe₂ ML, BL, TL, FL and bulk

In this section, we study the structural properties of the different PtSe₂ systems, namely ML, BL, TL, FL and bulk systems. The structural parameters in the z -direction are mainly governed by the vdW interaction. Therefore, to properly calculate these parameters, we consider different GGA+PBE+vdW corrections. In particular, we use vdW-DF [38], vdW-DF2 [39], rVV10 [40], DFT-D [41], and DFT-D3 [42] in order to obtain results in good agreement with those experimental observations. The calculated structural parameters are illustrated in Table (I). These parameters include the lattice parameters a and c , the inter-layer distance d_{int} , and the distance between two successive Pt atomic planes d_{Pt-Pt} as depicted in figure (1). The obtained results are compared with existing literature and experimental data for PtSe₂ crystal structures.

For the single PtSe₂ ML, our calculations are limited to the GGA approximation due to the absence of vdW out-of-plane interactions. A lattice parameter of $a = 3.73\text{\AA}$ and a monolayer thickness of $d_{Se-Se} = 2.68\text{\AA}$ were found. These values are in excellent agreement with previous theoretical results incorporating vdW corrections [26]. Moreover, they closely align with experimental observations [24]. Consequently, for the PtSe₂ ML, the conventional GGA approximation for the

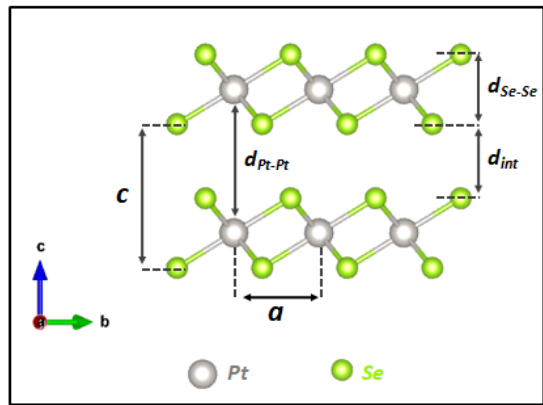


FIG. 1. Schematic representation of the crystal structure of PtSe₂ BL. The quantities a and c are the lattice parameters. The distance d_{int} is the interlayer distance between two successive layers of PtSe₂ systems. The distance d_{Se-Se} is the thickness of the layer, and d_{Pt-Pt} represents the distance between two successive Pt atomic planes.

exchange-correlation potential appears to be sufficient for accurately describing its crystal structure.

In the bulk case, the lattice parameter a is found around 3.7\AA for all the considered vdW corrections. This value is in good agreement with previous experimental [24, 86, 87], and theoretical results [24, 26, 86]. Unlike a parameter, both c and d_{int} are expected to change by enhancing the vdW interaction. However, the obtained c value for all corrections is around 4.7\AA which is in agreement with the previous calculations [24, 26, 86]. In fact, the theoretical approaches seem to underestimate the experimental value of $c = 5\text{\AA}$ [86–88]. In addition to c , the distance d_{int} remains almost fixed under the different vdW corrections. This may due to translation symmetry along the z -axis. The continued inter-layer interaction leaves the distance d_{int} unchanged. Our calculations highlight that the PtSe₂ bulk can not be affected by the introduction of the vdW corrections unlike the ML, BL, TL, and FL structures of PtSe₂. This result reveals the fundamental importance of transitional symmetry.

The broken perpendicular translation symmetry in the case of PtSe₂ BL, TL, and FL can lead to a change in d_{int} by considering the vdW corrections in the calculations. Indeed, the latter cases are freer to move along the axis (oz) and can be more influenced by vdW corrections. Therefore, by taking into account the vdW corrections, variations in the structural parameters of PtSe₂ BL, TL, and FL structures are found, as detailed in Table (I). In fact, the lattice parameter a remains almost unchanged. In contrast, the c parameter shows a decrease following the incorporation of vdW corrections. This reduction, obtained for PtSe₂ BL, TL, and FL systems, is mainly attributed to a decrease in

TABLE I. The structural parameters calculated for the PtSe₂ ML ML, BL, TL, FL, and bulk structures. In particular, the table shows the lattice constants a and c , the interlayer distance d_{int} , and the distance between Pt planes d_{Pt-Pt} for different vdW functionals.

System	Approach	a (Å)	c (Å)	d_{int} (Å)	d_{Pt-Pt} (Å)
PtSe ₂ ML	GGA	3.73	-	-	-
	DFT-D [26]	3.70	-	-	-
	DFT-D3 [69]	3.75	-	-	-
	Exp [24]	3.75	-	-	-
PtSe ₂ BL	GGA	3.73	6.52	3.89	6.52
	vdW-DF	3.73	5.79	3.03	5.77
	vdW-DF2	3.85	5.59	2.84	5.57
	rVV10	3.79	5.18	2.50	5.16
	DFT-D	3.73	4.75	2.12	4.69
	DFT-D3	3.73	5.45	2.81	5.44
	DFT-D3 [23]	3.77	4.82	-	4.92
	DFT-D [26]	3.73	4.76	2.14	-
	optB86b-vdW [84]	3.74	-	-	5.14
	Exp [23]	3.8	-	-	5±0.3
PtSe ₂ TL	GGA	3.74	6.00	3.40	6.00
	vdW-DF	3.81	5.62	2.95	5.61
	vdW-DF2	3.86	5.58	2.83	5.57
	rVV10	3.80	5.16	2.49	5.14
	DFT-D	3.74	4.72	2.11	4.76
	DFT-D3	3.74	5.46	2.69	5.45
	DFT-D [26]	3.74	4.72	2.14	-
	Exp [24]	-	-	-	5.9
PtSe ₂ FL	GGA	3.75	5.83	3.25	5.82
	vdW-DF	3.80	5.61	2.94	5.60
	vdW-DF2	3.86	5.57	2.83	5.56
	rVV10	3.81	5.12	2.46	5.11
	DFT-D	3.75	4.69	2.11	4.68
	DFT-D3	3.77	5.28	2.69	5.27
	DFT-D[26]	-	-	-	-
Exp [24]	-	-	-	5.8	
Bulk PtSe ₂	GGA	3.76	4.67	2.13	4.67
	vdW-DF	3.77	4.68	2.11	4.68
	vdW-DF2	3.77	4.68	2.07	4.68
	rVV10	3.77	4.68	2.11	4.68
	DFT-D	3.77	4.68	2.13	4.68
	DFT-D3	3.77	4.69	2.16	4.69
	DFT-D3 [24]	3.775	4.802	-	-
	DFT-D[26]	3.77	4.70	-	-
	GGA [24]	3.759	6.121	-	-
	optB88-vdW [86]	3.785	4.969	-	-
	Exp [24]	3.75	5.6	-	-
Exp [87]	3.727	5.07±0.01	-	-	
Exp [88]	3.82	5.08	-	-	
Exp [86]	3.728	5.081	-	-	

the distance d_{int} . Indeed, the attraction between the layers is strengthened by these corrections, resulting in a decrease in the distance d_{int} and, consequently, in the lattice constant c . It is therefore important to take into account the vdW corrections in order to obtain an accurate description of the crystal structure of PtSe₂ BL, TL and FL.

Furthermore, based on Table I, while the distances

c and d_{Pt-Pt} are equal in the case of bulk, the lattice parameter c becomes larger than d_{Pt-Pt} in the case of PtSe₂ BL, TL, and FL materials. This is explained by the fact that the Se planes in each layer lose the symmetry with respect to Pt plane. After ion relaxation, some of them becomes closer to Pt planes than the others. This asymmetric behavior leads to difference between the distances d_{Pt-Pt} and c . Continuing our comparison between the PtSe₂ bulk and the rest of layered

PtSe₂ systems, the parameters c and d_{int} are plotted as a function of the different structure in figure (2). In fact, the main difference between the bulk and the rest is c and d_{int} parameters. In particular, for all DFT+vdW corrections except DFT+DFT-D, by reducing the number of layers to BL and TL, d_{int} and c becomes slightly larger. Therefore, the inter-layer coupling is more pronounced in the bulk.

Furthermore, the results given by DFT+vdW corrections are different from each other. On the one hand, table (I) shows that the DFT+DFT-D method gives the smallest inter-layer distance. This can be explained by the fact that the DFT+DFT-D method often overestimates vdW interaction [42, 89]. On the other hand, the DFT+vdW-DF correction underestimates this interaction due to the repulsive nature of the Perdew-Burke-Ernzerhof exchange functional (revPBE) [90, 91]. For this reason, the DFT+vdW-DF method presents the largest value of the distance d_{int} . Furthermore, the DFT+vdW-DF methods lead to a d_{Pt-Pt} distance in good agreement with the experimental work of Zhang *et al.* [24] for PtSe₂ BL and TL. However, for the same lattice parameter d_{Pt-Pt} , the DFT+rVV10 approach gives a closer result to the experiment of Li *et al.* [23]. For this reason, we will use DFT+rVV10 approach in the following calculations.

B. Electronic structure of PtSe₂

1. Effect of the layer number on PtSe₂ band structure

One of the most important characteristics of TMD is the variation of their electronic properties with respect to the number of layers. The PtSe₂ material stands out among the other TMD by a transition from a semi-metallic material in the bulk to a semiconductor material for a small number of layers. The challenge is to deeply understand the correlation between the number of layers and the SM-SC transition. In this section, the band structures are calculated and presented for the different PtSe₂ systems, in particular ML, BL, TL, FL and bulk PtSe₂ materials. Our method uses the GGA and GGA plus vdW corrections in order to determine this SM-SC transition. Here, the energy dispersion of the different systems are calculated for the in-plane wave vector of the first Brillouin zone (FBZ). Indeed, the considered high-symmetry path is K- Γ -M-K as illustrated in figure 3.

As shown in figure (5), PtSe₂ ML exhibits a semiconductor character with a bandgap (E_g) of 1.30 eV in both the DFT and DFT+vdW approximations. As discussed in previous section, vdW corrections have no effect on the properties of PtSe₂ ML. The valence band maximum of PtSe₂ ML is located at Γ point, while the conduction band minimum is located between

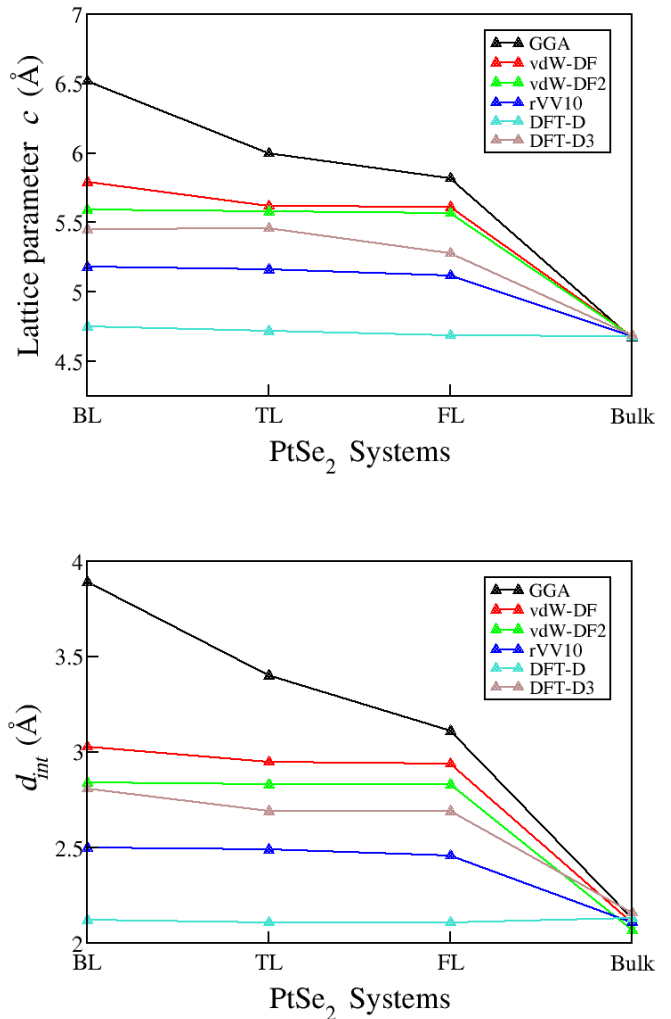


FIG. 2. The lattice parameter c and the inter-layer distance d_{int} as a function of the number of layers of PtSe₂ for GGA and GGA+vdW approximations.

Γ and M points. The valence band shows an almost flat dispersion around Γ point. This shape has been experimentally observed using Angle-Resolved Photoemission Spectroscopy (ARPES) [30]. The indirect bandgap has been observed in group 10 TMD monolayers (such as PtSe₂, PdSe₂...) unlike the group 6 TMD monolayers (MoS₂, WSe₂...) which exhibit a direct bandgap [12, 92, 93]. Consequently, the optical transition requires the involvement of phonons to ensure the conservation of electron momentum. This categorizes PtSe₂ ML as a poor emitter and absorber of light [94, 95].

According to the figure (4), the bandgap of PtSe₂ BL, TL, or FL depends on the used vdW correction. Under the GGA approximation, E_g is maximal and equal to 1 eV, 0.67 eV, and 0.48 eV for PtSe₂ BL, TL and FL,

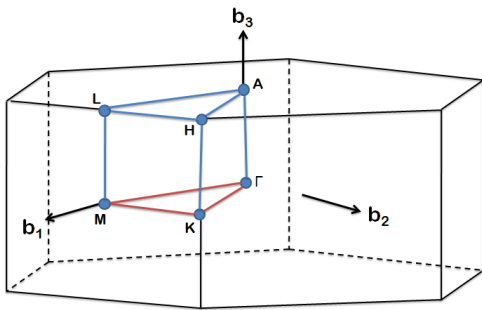


FIG. 3. First Brillouin zone in the reciprocal space of the PtSe₂. The line of high symmetry used for the study of the structure of the bands (red).

respectively. However, the bandgap decreases, and even vanishes when vdW corrections are introduced. This reduction in the bandgap under the influence of vdW corrections is related to the attraction enhancement between PtSe₂ layers. In particular, the vdW corrections take into account the long range correlation which leads to the closing of the bandgap. Despite this fact, PtSe₂ BL maintains its semiconductor character in all used vdW approximations.

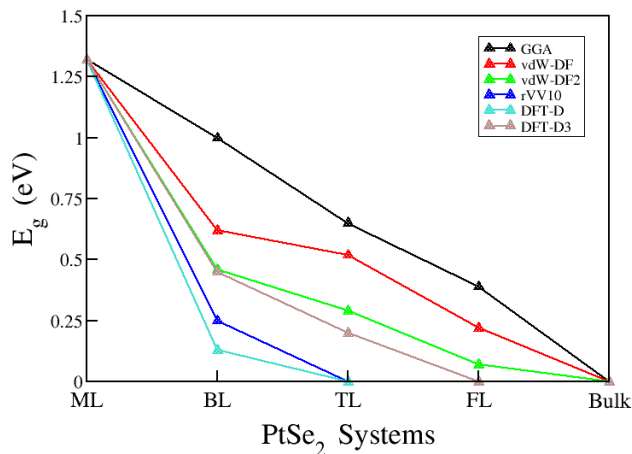


FIG. 4. The bandgap values of the various PtSe₂ systems for all the considered exchange-correlation approximations.

Furthermore, figure (4) shows that PtSe₂ TL exhibits a semi-metallic character for the two corrections DFT+rVV10 and DFT+DFT-D, which is consistent with experimental data from reference [23]. However, according to the DFT+vdW-DF, DFT+vdW-DF2, and DFT+DFT-D3 approximations, PtSe₂ TL displays a semiconductor behavior with a smaller bandgap than that obtained in the GGA approximation. This result is in agreement with the experimental observations from reference [24]. This discrepancy stems mainly from

the interlayer distance and c constant where relatively larger d_{int} leads to semiconductor character. Indeed, according to table (II), these distances are found larger in the case of DFT+vdW-DF, DFT+vdW-DF2, and DFT+DFT-D3 calculations. Interestingly, the difference between the DFT+DFT-D3 and DFT+rVV10 interlayer distances is equal to 0.20 Å, which reflecting the gap sensitivity to d_{int} .

The interlayer distance effect on the electronic properties can explain the difference between the results of the two experiments in Refs. [23, 24]. In [23], the SC-SM transition was observed at the third layer. However, in Ref. [24], the transition happened at the fifth layer. Indeed, this discrepancy between both experiments, can be attributed to the difference in the interlayer distance d_{int} . In fact, while a distance d_{Pt-Pt} of 5 ± 0.3 Å was assigned in Ref. [23], the experiment in Ref. [24] shows a distance around 5.6 Å. The increasing in the bandgap is directly related to the increase in the interlayer distance, leading to transitions occurring in higher layers. The observed difference in the distance d_{Pt-Pt} between the two experiments may due to the growth protocols, experimental conditions. The high sensitivity to the interlayer distance suggest that the SM-SC transition in PtSe₂ material is not unique for a given layer number.

TABLE II. Comparison of PtSe₂ ML, BL, TL, FL bandgap energies obtained by applying different theoretical functionals and observed in different experiments.

Approach	ML	BL	TL	FL	Bulk
GGA	1.30	1.09	0.67	0.48	0
vdW-DF	1.30	0.62	0.53	0.22	0
vdW-DF2	1.30	0.42	0.21	0.07	0
rVV10	1.30	0.25	0	0	0
DFT-D	1.30	0.12	0	0	0
DFT-D3	1.30	0.45	0.20	0	0
DFT-D [26]	1.17	0.17	0	0	0
DFT-D3 [69]	1.39	0.99	-	-	0
optB88-vdW [86]	1.18	0.21	0	0	0
GGA [23]	1.20	0.22	0.01	0	0
GGA [31]	1.60	0.8	-	-	0
G ₀ W ₀ [96]	2.10	-	-	-	0
G ₀ W ₀ [23]	2.44	1.174	0.30	0	0
HSE06 [24]	1.837	0.796	0.417	0.148	0
LDA [84]	1.2	0.21	0	0	0
Exp [23]	1.8	0.6	0	0	0
Exp [24]	2.0	1.1	0.6	0.2	0

A zero bandgap corresponds to the semi-metallic nature

In Table II, we present the bandgap values obtained from our DFT calculations for the various PtSe₂ systems in comparison with previous theoretical and experimental results. For the case of the PtSe₂ ML, while the GGA, LDA, and GGA+vdW approximations underestimate the experimental bandgap values, the GW approximation overestimate it. In the case of PtSe₂ BL and TL, our GGA and GGA+vdW-DF calculations give a good

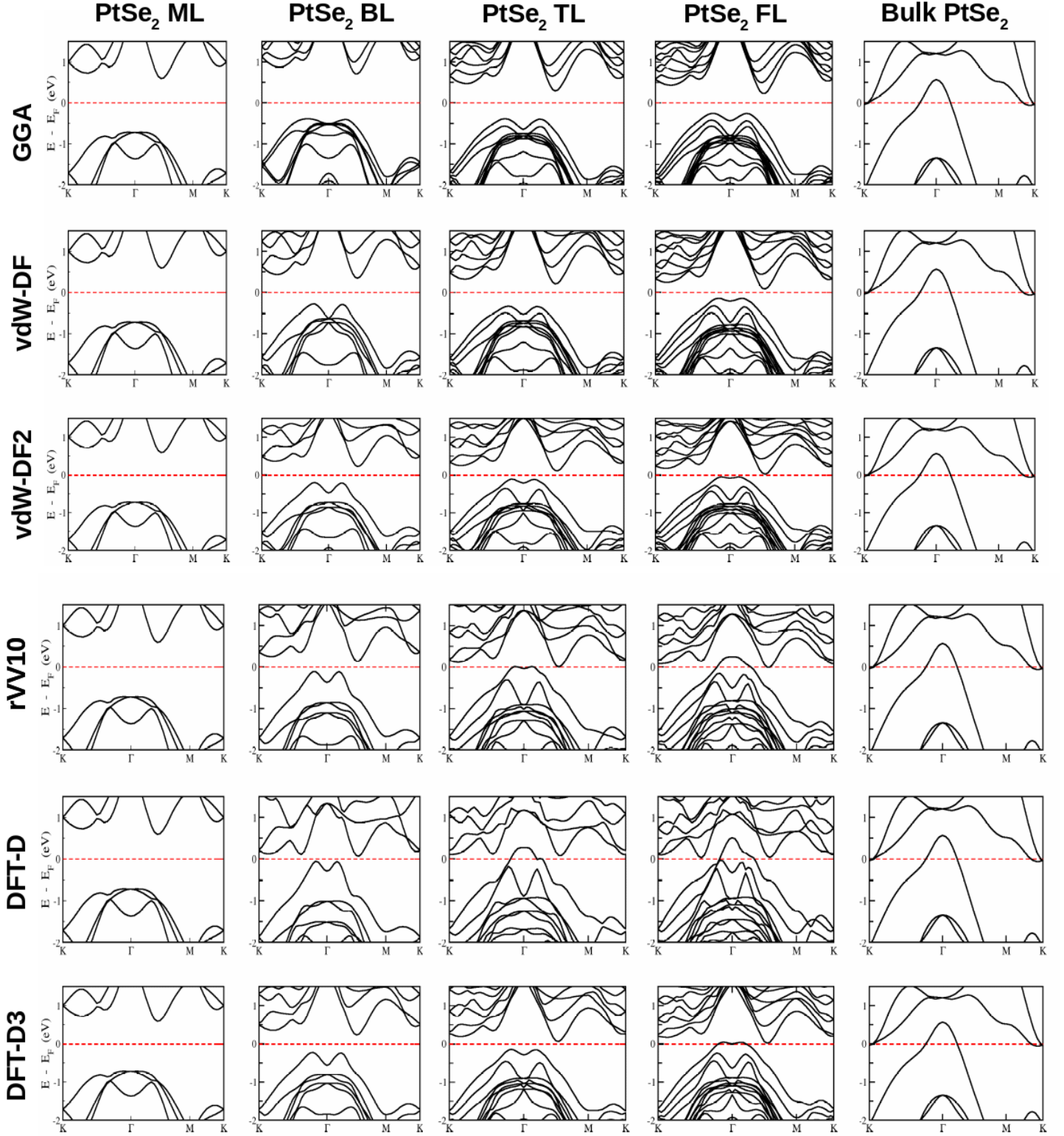


FIG. 5. Band structures of the different PtSe₂ systems (ML, BL, TL, FL and bulk) with GGA approximation and vdW corrections. The Fermi level is considered as the origin of the energy.

agreements with the experiments of Refs. [23, 24]. However, these exchange-correlation approximations did not lead to a SM-SC transition in contradiction with the experiment [23]. Furthermore, in the case of TL and FL, while GGA+rVV10 and DFT-D calculations are in good agreement the observed values in Ref. [23], GGA+vdW-DF method gives a close bandgap energies to that of the experiment [24], which is consistent with the obtained agreement for d_{Pt-Pt} (see table I). Overall, while the obtained results of GGA+vdW-DF method are in agreement with the experiment of Zhang *et al.* [24], the calculated results of GGA+rVV10 approach are close that of the experiment of Li *et al.* [23].

2. The effect of the distance d_{int} on the bandgap of PtSe₂ structures

In order to compare the bandgap variation of different layered structures, namely PtSe₂ BL, TL, and FL, the bandgap energy as a function of d_{int} is plotted in Figure (6). Note that the chosen value of d_{int} goes from 2.5 to 4 Å which covers all the values found by the different corrections. As expected, for each of these systems, the bandgap energy increases as the interlayer distance increases. However, for PtSe₂ BL, the bandgap shows the highest bandgap values compared to TL and FL systems. Therefore, the effect of the interlayer distance is more pronounced in the case of BL.

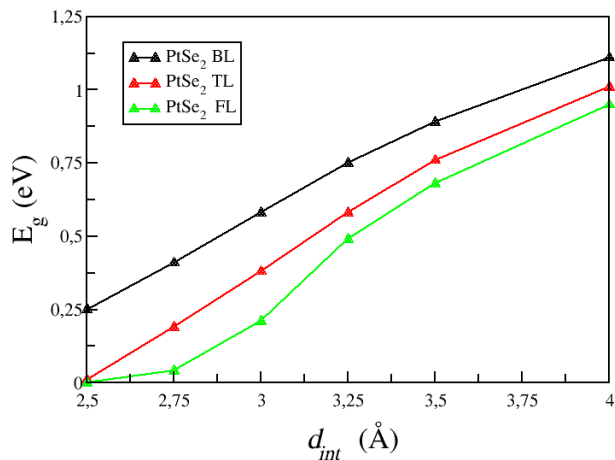


FIG. 6. Variation of the bandgap as a function of the distance d_{int} based on the GGA+rVV10 method.

The sensitivity of the bandgap to interlayer separation suggests that the distance d_{int} can be adjusted through vertical compressive strain along the (oz) axis. This approach can be applied to the case of PtSe₂ BL which the best candidate to illustrate the effect of this strain. A detailed analysis of the strain effect on PtSe₂ BL is

provided in the third part of this article.

3. Origin of the SM-SC transition

In order to further explore the origin of the SM-SC transition, we calculated the projected band structures for the different layered systems (see figure (7)), using GGA+rVV10 approximation. In PtSe₂ ML, the maximum of the valence band (VBM) is mainly constituted by the p_y orbitals of the chalcogen atom Se. Besides, the conduction band (CB) is essentially constructed by both p_y and p_z orbitals of the Se atom. As the number of layers increases, moving from PtSe₂ ML to bulk material, an interesting change occurs. The p_z orbitals rises above the p_y orbitals and takes on a higher energy, while the p_y orbitals retains almost the same position and energy. For the conduction band, the doublet of the p_y and p_z orbitals moves to a lower energy level, until the overlap with the p_z orbitals of the valence band. This highlights the sensitivity of the p_z orbitals to interactions between the layers in the material. Therefore, the origin behind the SM-SC transition is mainly the evolution of p_z orbitals.

C. Strain effect on PtSe₂ BL

The sensitivity to the interlayer distance open the possibility of tuning the bandgap of PtSe₂ BL. In fact, a way of controlling the interlayer distance is by applying a vertical compressive strain. Indeed, in Ref. [69], this strain was applied by changing and constraining the interlayer distance. Here, the strain was defined as $\epsilon = \frac{(d_0-d)}{d_0}$, where d and d_0 are the interlayer distance with and without strain, respectively. In this picture, the in-plane parameters are kept unchanged. In fact, in order to optimize the BL structure, the supercell approach should be considered to treat the non-periodicity along z direction. However, this fact make impossible to control c parameter of the BL. In our work, we present a fully optimized structure method. Indeed, the BL structure is optimized after the application of strain ϵ which is defined as,

$$\epsilon = \frac{(c - c')}{c'} \quad (1)$$

where c and c' are the BL lattice parameter without and with strain, respectively. In order to optimize the BL structure, a two step approach was adopted. First, an in-plane optimization is performed for the bulk PtSe₂ material. Here, we consider the following approximation,

$$c' = c^{Bulk}(xy) \simeq c^{BL}(L \rightarrow \infty) \quad (2)$$

Here, c' is equal to the lattice parameter of the bulk $c^{Bulk}(xy)$ for an in-plane optimization, where L is the vacuum width of BL supercell. For each strain the c^{Bulk} is fixed only the in-plane parameters such as d_{int}

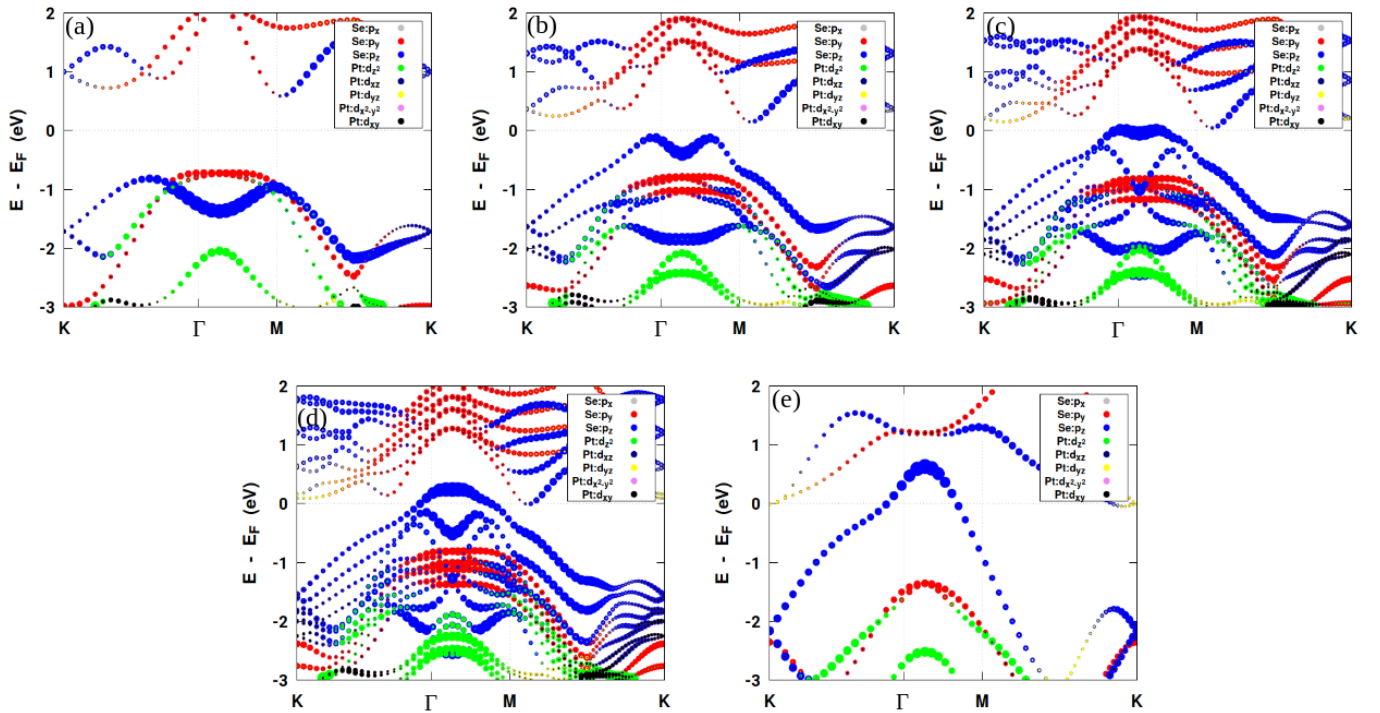


FIG. 7. Projected Band Structures for different PtSe₂ Systems (ML(a), BL(b), TL(c), FL(d) and Bulk(e)), using rVV10 correction.

and a are allowed to move. For instance, in the case of unstrained BL, by fixing c^{Bulk} to $c^{BL} = 5.18 \text{ \AA}$, the calculated parameter of the bulk after an in-plane optimization, $a^{Bulk} = 3.8 \text{ \AA}$ and $d_{int}^{Bulk} = 2.51 \text{ \AA}$ are almost equal to the parameters $a^{BL} = 3.79 \text{ \AA}$ and $d_{int}^{BL} = 2.50 \text{ \AA}$ of the BL. In the second step, for a given strain, the in-plane optimized parameters, a^{Bulk} and d_{int}^{Bulk} , used together with the supercell approach, we calculate the band structure of the strained BL.

By applying vertical compressive strain to the PtSe₂ BL, a variations in structural parameters is induced, namely in the distances a and the d_{int} , as depicted in figure (8). The distance d_{int} consistently decreases as the applied strain increases, with a reduction exceeding 0.40 \AA for a compression of $\epsilon = 15\%$. This corresponds to a reduction of 0.77 \AA for the distance c . In contrast to d_{int} , the parameter a experiences a relatively modest increase. For an unstrained structure, the parameter a is 3.79 \AA , while with a strain of $\epsilon = 15\%$, it reaches 3.96 \AA . This slight increase in parameter a is attributed to the system ability to freely relax within the (xy) plane, constantly seeking the ground state of energy.

In order to reveal the influence of the vertical compressive strain on the bandgap and the band structure, we plot figures (9) and (11), respectively. In particular, according to figure (9), the increase in ϵ leads to the decrease of the bandgap energy. Indeed, in the range of $\epsilon = 1\%$ to 16% , PtSe₂ BL maintains its semiconductor

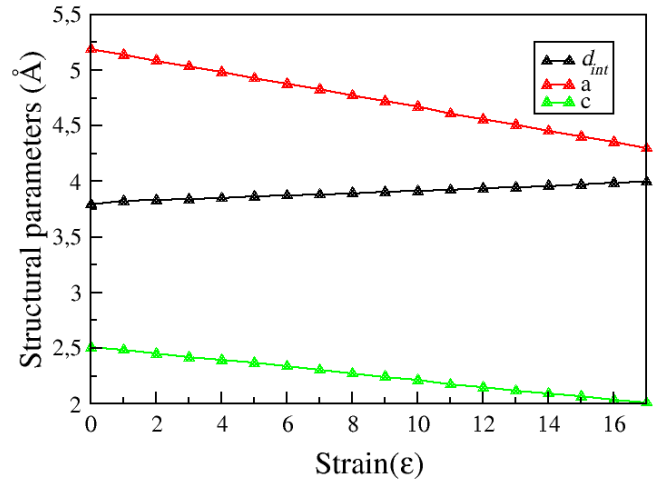


FIG. 8. Evolution of structural parameters a , c , and d_{int} as a function of vertical compressive strain for PtSe₂ BL.

character, with a decrease in the bandgap energy ranging from 0.25 eV to 0.01 eV . The bandgap varies with a step of approximately $-0.02 \text{ eV}/1\%$, which is of the same order of magnitude as the experimental results obtained for the monolayer MoSe₂ under vertical compressive strain, approximately $-27 \pm 2/1\%$ [25]. Note that, for a vertical strain lower than 8% , the bandgap

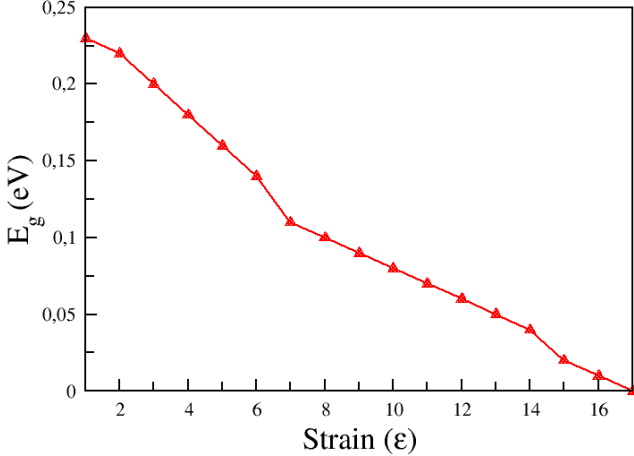


FIG. 9. bandgap of the PtSe₂ BL as a function of the vertical compressive strain.

becomes narrow and less than 0.1 eV. From $\epsilon = 17\%$, the PtSe₂ BL adopts a semi-metallic character, exhibiting a negative bandgap. Therefore, the strain offer the possibility of reversibly tuning the BL bandgap by about 0.25 eV through application. The reduction of the bandgap energy under vertical compressive strain was also found by *Li et al.* [69]. However, in this reference, the SM-SC transition was assigned to a large strain of over 40%, where the bandgap goes from 1 to 0 eV. This discrepancy is due to the use of different vdW correction and the in-plane optimization in our calculations of strained BL.

To evaluate the applied pressure to the PtSe₂ BL under strain, we present in the figure (10) the calculated pressure for each level of strain, using the formula $P = (E_0^{tot} - E^{tot}) / ((c - c') \times A)$ [69, 97, 98]. The terms E_0^{tot} and E^{tot} represent the total energies of the systems without and under strain, respectively, and A represents the surface of the primitive cell of the strained system. Our results indicate that the pressure is ranging from 1 GPa to 7.7 GPa. The pressure needed for the SC-SM transition is 7.7 GPa which larger than the values obtained in Ref. [17, 69]. In fact, this pressure is lower than that found in the case of PtSe₂ ML to achieve its semi-metallic character under in-plane strain [57]. Indeed, for PtSe₂ ML [57], a strain of 8% was found to induce an SC-SM transition, requiring a pressure exceeding 10 GPa.

Furthermore, the band structures of strained BL are shown in figure (11). The increase of the strain leads to energy shift in the valence and conduction bands. Besides, under the effect of the strain, a new band parabolic dispersion appears, in the valence band near

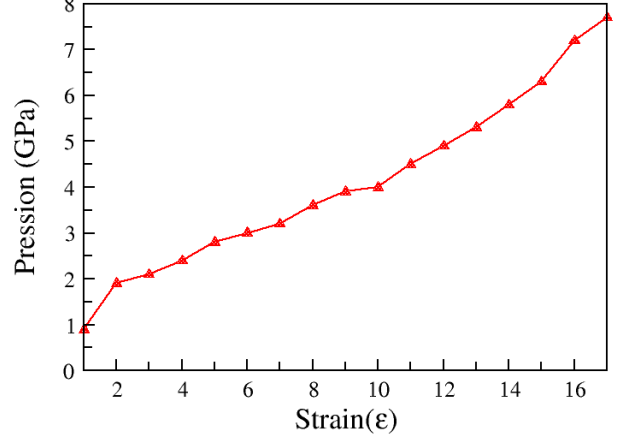


FIG. 10. Applied pressure per unit cell of PtSe₂ BL as a function of the vertical compressive strain (ϵ).

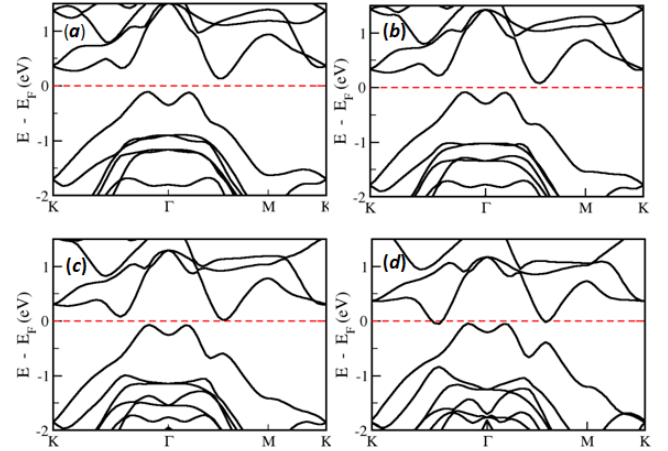


FIG. 11. Band structures of PtSe₂ BL for Strain $\epsilon = 1\%$ (a), $\epsilon = 5\%$ (b), $\epsilon = 10\%$ (c), and $\epsilon = 17\%$ (d), using GGA+rVV10 functional.

M point. Moreover, the lower valence band loses its flat form. To further understand the effect of the strain on the electronic bands, we plot the projected band structures in figure (12). The indicated modifications in the band structure under vertical compressive strain, stem mainly from p_z orbitals of Se atom. In fact, the interlayer interaction is enhanced due to the applied strain leading the valence band dominated by p_z orbital to shift toward higher energy. Meanwhile, the bands dominated in-plane p_x and p_y orbital contribution of Se atom remain almost unchanged.

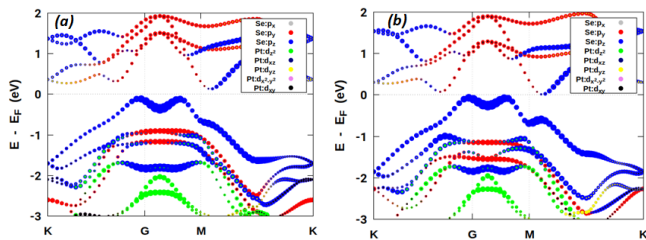


FIG. 12. Projected band structures for the PtSe₂ BL under a 1% strain (a) and a 10% strain (b).

IV. CONCLUSIONS

In this work, we presented an investigation of the structural and electronic properties of the PtSe₂ ML, BL, TL, FL, bulk and strained BL using first principle calculations. In order to treat the vdW interactions between PtSe₂ layers, the functionals GGA, GGA+vdW-DF, GGA+vdW-DF2, GGA+rVV10, GGA+DFT-D and GGA+DFT-D3 were adopted. The structure optimisation revealed that by reducing the number of layers, the parameter c and the interlayer distance d_{int} increase. For instance, the d_{int} (c) goes from 2.11 Å (4.68 Å) in the bulk to 2.50 Å (5.18 Å) in BL. In addition, our findings of crystal structure show that unlike PtSe₂ bulk, the vdW corrections are important in the case of BL, TL and FL. Indeed, while the crystal parameters c and d_{int} remain unchanged in the case of the Bulk, they de-

creases in the case of BL, TL and FL systems. This is due to the enhancement of interlayer interaction and the brooking out-of-plane periodicity by including the vdW corrections. Therefore, our results reveal the importance of vdW interactions in the case of few-layer systems. Furthermore, regarding the electronic proprieties of PtSe₂, the SM-SC transition is found depending on the considered vdW corrections. In fact, the origin of this dependence is the high sensitivity to the variation of interlayer distance. Indeed, a change of 0.2 Å in the interlayer distance in the case of the PtSe₂ TL was found enough the change its character from semi-conductor to semi-metal. Therefore, this distance plays a key role for the electronic properties of PtSe₂ material, serving as the origin of the SC-SM transition. More precisely, the SC-SM transition in PtSe₂ material originates from the energy shift of Se- p_z dominated conduction and valence bands. Our results reveal that the exact determination of the SM-SC transition in this material is challenging and can be different from one experiment to another. Due to the interlayer distance effect, applying an vertical compressive strain represent an effective tool to tune the bandgap of PtSe₂ material. In particular, the PtSe₂ BL show the highest sensitivity to the d_{int} among the other considered systems. Hence, by applying a vertical compressive strain from 1 to 16%, the bandgap decreased from 0.25 to 0.01 eV. The SM-SC transition was obtained at 17% due to the decrease of the interlayer distance. The bandgap tuning of PtSe₂ BL under vertical compressive strain is of particular interest in the development and fabrication of optoelectronics nanodevices.

-
- [1] W. Choi, N. Choudhary, G. H. Han, J. Park, D. Akinwande, and Y. H. Lee, Recent development of two-dimensional transition metal dichalcogenides and their applications, *Materials Today* **20**, 116 (2017).
 - [2] W. Alfalasi, Y. P. Feng, and N. Tit, Designing a functionalized 2d-tmd (mox₂, x= s, se) hosting half-metallicity for selective gas-sensing applications: Atomic-scale study, *Acta Materialia* **246**, 118655 (2023).
 - [3] S. Z. Butler, S. M. Hollen, L. Cao, Y. Cui, J. A. Gupta, H. R. Gutiérrez, T. F. Heinz, S. S. Hong, J. Huang, A. F. Ismach, *et al.*, Progress, challenges, and opportunities in two-dimensional materials beyond graphene, *ACS nano* **7**, 2898 (2013).
 - [4] Q. H. Wang, K. Kalantar-Zadeh, A. Kis, J. N. Coleman, and M. S. Strano, Electronics and optoelectronics of two-dimensional transition metal dichalcogenides, *Nature nanotechnology* **7**, 699 (2012).
 - [5] H. Mu, Z. Wang, J. Yuan, S. Xiao, C. Chen, Y. Chen, Y. Chen, J. Song, Y. Wang, Y. Xue, *et al.*, Graphene-bi2te3 heterostructure as saturable absorber for short pulse generation, *Acs Photonics* **2**, 832 (2015).
 - [6] J. Liu, Z. Hu, Y. Zhang, H.-Y. Li, N. Gao, Z. Tian, L. Zhou, B. Zhang, J. Tang, J. Zhang, *et al.*, Mos₂ nanosheets sensitized with quantum dots for room-temperature gas sensors, *Nano-Micro Letters* **12**, 1 (2020).
 - [7] D. Li, Y. Gong, Y. Chen, J. Lin, Q. Khan, Y. Zhang, Y. Li, H. Zhang, and H. Xie, Recent progress of two-dimensional thermoelectric materials, *Nano-Micro Letters* **12**, 1 (2020).
 - [8] Z. Kang, Y. Cheng, Z. Zheng, F. Cheng, Z. Chen, L. Li, X. Tan, L. Xiong, T. Zhai, and Y. Gao, Mos₂-based photodetectors powered by asymmetric contact structure with large work function difference, *Nano-micro letters* **11**, 1 (2019).
 - [9] A. K. Mia, M. Meyyappan, and P. Giri, Two-dimensional transition metal dichalcogenide based biosensors: From fundamentals to healthcare applications, *Biosensors* **13**, 169 (2023).
 - [10] Y. Shi, H. Li, and L.-J. Li, Recent advances in controlled synthesis of two-dimensional transition metal dichalcogenides via vapour deposition techniques, *Chemical Society Reviews* **44**, 2744 (2015).
 - [11] L. Pi, L. Li, K. Liu, Q. Zhang, H. Li, and T. Zhai, Recent progress on 2d noble-transition metal dichalcogenides, *Advanced Functional Materials* **29**, 1904932 (2019).
 - [12] A. D. Oyedele, S. Yang, L. Liang, A. A. Puretzky, K. Wang, J. Zhang, P. Yu, P. R. Pudasaini, A. W. Ghosh, Z. Liu, *et al.*, Pdse₂: pentagonal two-dimensional layers with high air stability for electronics, *Journal of the*

- American Chemical Society **139**, 14090 (2017).
- [13] Y. Gong, Z. Lin, Y.-X. Chen, Q. Khan, C. Wang, B. Zhang, G. Nie, N. Xie, and D. Li, Two-dimensional platinum diselenide: synthesis, emerging applications, and future challenges, *Nano-Micro Letters* **12**, 1 (2020).
- [14] I. Setiyawati, K.-R. Chiang, H.-M. Ho, and Y.-H. Tang, Distinct electronic and transport properties between 1t-hfse₂ and 1t-ptse₂, *Chinese Journal of Physics* **62**, 151 (2019).
- [15] S. Wagner, C. Yim, N. McEvoy, S. Kataria, V. Yokaribas, A. Kuc, S. Pindl, C.-P. Fritzen, T. Heine, G. S. Duesberg, *et al.*, Highly sensitive electromechanical piezoresistive pressure sensors based on large-area layered ptse₂ films, *Nano letters* **18**, 3738 (2018).
- [16] G. Wang, Z. Wang, N. McEvoy, P. Fan, and W. J. Blau, Layered ptse₂ for sensing, photonic, and (opto-)electronic applications, *Advanced Materials* **33**, 2004070 (2021).
- [17] W. Lei, R. Hu, S. Han, H. Yuan, W. Jiao, Y. Luo, and H. Liu, Directional control of the electronic and phonon transport properties in the ferroelastic ptse₂, *The Journal of Physical Chemistry C* (2023).
- [18] M. Hemmat, S. Ayari, M. Mićica, H. Vergnet, S. Guo, M. Arfaoui, X. Yu, D. Vala, A. Wright, K. Postava, *et al.*, Layer-controlled nonlinear terahertz valleytronics in two-dimensional semimetal and semiconductor ptse₂, *InfoMat*, e12468 (2023).
- [19] M. Tharrault, S. Ayari, E. Desgué, M. Arfaoui, R. L. Goff, P. Morfin, J. Palomo, M. Rosticher, S. Jaziri, B. Plaçais, *et al.*, The optical absorption in indirect semiconductor to semimetal ptse₂ arises from direct transitions, *arXiv preprint arXiv:2311.01847* (2023).
- [20] Y. Zhao, J. Qiao, Z. Yu, P. Yu, K. Xu, S. P. Lau, W. Zhou, Z. Liu, X. Wang, W. Ji, *et al.*, High-electron-mobility and air-stable 2d layered ptse₂ fets, *Advanced Materials* **29**, 1604230 (2017).
- [21] A. AlMutairi, D. Yin, and Y. Yoon, Ptse₂ field-effect transistors: New opportunities for electronic devices, *IEEE Electron Device Letters* **39**, 151 (2017).
- [22] D. Wu, Y. Wang, L. Zeng, C. Jia, E. Wu, T. Xu, Z. Shi, Y. Tian, X. Li, and Y. H. Tsang, Design of 2d layered ptse₂ heterojunction for the high-performance, room-temperature, broadband, infrared photodetector, *Acs Photonics* **5**, 3820 (2018).
- [23] J. Li, S. Kolekar, M. Ghorbani-Asl, T. Lehnert, J. Biskupek, U. Kaiser, A. V. Krashennnikov, and M. Batzill, Layer-dependent band gaps of platinum dichalcogenides, *ACS Nano* **15**, 13249 (2021).
- [24] L. Zhang, T. Yang, M. F. Sahdan, Arramel, W. Xu, K. Xing, Y. P. Feng, W. Zhang, Z. Wang, and A. T. Wee, Precise layer-dependent electronic structure of mbe-grown ptse₂, *Advanced Electronic Materials* **7**, 2100559 (2021).
- [25] J. O. Island, A. Kuc, E. H. Diependaal, R. Bratschitsch, H. S. Van Der Zant, T. Heine, and A. Castellanos-Gomez, Precise and reversible band gap tuning in single-layer mose₂ by uniaxial strain, *Nanoscale* **8**, 2589 (2016).
- [26] A. Kandemir, B. Akbali, Z. Kahraman, S. Badalov, M. Ozcan, F. İyikanat, and H. Sahin, Structural, electronic and phononic properties of ptse₂: from monolayer to bulk, *Semiconductor Science and Technology* **33**, 085002 (2018).
- [27] M. Yan, E. Wang, X. Zhou, G. Zhang, H. Zhang, K. Zhang, W. Yao, N. Lu, S. Yang, S. Wu, *et al.*, High quality atomically thin ptse₂ films grown by molecular beam epitaxy, *2D Materials* **4**, 045015 (2017).
- [28] L. Ansari, S. Monaghan, N. McEvoy, C. Ó. Coileáin, C. P. Cullen, J. Lin, R. Siris, T. Stimpel-Lindner, K. F. Burke, G. Mirabelli, *et al.*, Quantum confinement-induced semimetal-to-semiconductor evolution in large-area ultra-thin ptse₂ films grown at 400° c, *npj 2D Materials and Applications* **3**, 33 (2019).
- [29] D. Dai, H.-J. Koo, M.-H. Whangbo, C. Soulard, X. Rocquefelte, and S. Jobic, Trends in the structure and bonding in the layered platinum dioxide and dichalcogenides ptq₂ (q= o, s, se, te), *Journal of Solid State Chemistry* **173**, 114 (2003).
- [30] Y. Wang, L. Li, W. Yao, S. Song, J. Sun, J. Pan, X. Ren, C. Li, E. Okunishi, Y.-Q. Wang, *et al.*, Monolayer ptse₂, a new semiconducting transition-metal-dichalcogenide, epitaxially grown by direct selenization of pt, *Nano letters* **15**, 4013 (2015).
- [31] M. O'Brien, N. McEvoy, C. Motta, J.-Y. Zheng, N. C. Berner, J. Kotakoski, K. Elibol, T. J. Pannycook, J. C. Meyer, C. Yim, *et al.*, Raman characterization of platinum diselenide thin films, *2D Materials* **3**, 021004 (2016).
- [32] M. Zulfqar, Y. Zhao, G. Li, S. Nazir, and J. Ni, Tunable conductivity and half metallic ferromagnetism in monolayer platinum diselenide: a first-principles study, *The Journal of Physical Chemistry C* **120**, 25030 (2016).
- [33] K. Ren, M. Sun, Y. Luo, S. Wang, Y. Xu, J. Yu, and W. Tang, Electronic and optical properties of van der waals vertical heterostructures based on two-dimensional transition metal dichalcogenides: First-principles calculations, *Physics Letters A* **383**, 1487 (2019).
- [34] V. Selamneni and P. Sahatiya, Mixed dimensional transition metal dichalcogenides (tmds) vdW heterostructure based photodetectors: a review, *Microelectronic Engineering* **269**, 111926 (2023).
- [35] E. Khestanova, T. Ivanova, R. Gillen, A. D'Elia, O. N. Gallego Lacey, L. Wysocki, A. Gruneis, V. Kravtsov, W. Strupinski, J. Maultzsch, *et al.*, Robustness of momentum-indirect interlayer excitons in mos₂/wse₂ heterostructure against charge carrier doping, *ACS Photonics* **10**, 1159 (2023).
- [36] J. J. Thompson, V. Lumsargis, M. Feierabend, Q. Zhao, K. Wang, L. Dou, L. Huang, and E. Malic, Interlayer exciton landscape in ws₂/tetracene heterostructures, *Nanoscale* **15**, 1730 (2023).
- [37] X. Zhen, H. Liu, F. Liu, S. Zhang, J. Zhong, and Z. Huang, Effect of s vacancy and interlayer interaction on the electronic and optical properties of mos₂/wse₂ heterostructure, *Journal of Electronic Materials* **52**, 1186 (2023).
- [38] K. Berland, V. R. Cooper, K. Lee, E. Schröder, T. Thonhauser, P. Hyldgaard, and B. I. Lundqvist, van der waals forces in density functional theory: a review of the vdw-df method, *Reports on Progress in Physics* **78**, 066501 (2015).
- [39] K. Lee, É. D. Murray, L. Kong, B. I. Lundqvist, and D. C. Langreth, Higher-accuracy van der waals density functional, *Physical Review B* **82**, 081101 (2010).
- [40] R. Sabatini, T. Gorni, and S. De Gironcoli, Nonlocal van der waals density functional made simple and efficient, *Physical Review B* **87**, 041108 (2013).
- [41] S. Grimme, Accurate description of van der waals complexes by density functional theory including empirical

- corrections, *Journal of computational chemistry* **25**, 1463 (2004).
- [42] J. Moellmann and S. Grimme, Dft-d3 study of some molecular crystals, *The Journal of Physical Chemistry C* **118**, 7615 (2014).
- [43] H. Peng, Z.-H. Yang, J. Sun, and J. P. Perdew, Scan+rvv10: A promising van der waals density functional, arXiv preprint arXiv:1510.05712 (2015).
- [44] F. Chiter, V. B. Nguyen, N. Tarrat, M. Benoit, H. Tang, and C. Lacaze-Dufaure, Effect of van der waals corrections on dft-computed metallic surface properties, *Materials Research Express* **3**, 046501 (2016).
- [45] R. L. Freire, D. Guedes-Sobrinho, A. Kiejna, and J. L. Da Silva, Comparison of the performance of van der waals dispersion functionals in the description of water and ethanol on transition metal surfaces, *The Journal of Physical Chemistry C* **122**, 1577 (2018).
- [46] R. Sabatini, E. Küçükbenli, C. H. Pham, and S. de Gironcoli, Phonons in nonlocal van der waals density functional theory, *Physical Review B* **93**, 235120 (2016).
- [47] Z. Dai, L. Liu, and Z. Zhang, Strain engineering of 2d materials: issues and opportunities at the interface, *Advanced Materials* **31**, 1805417 (2019).
- [48] L. Sortino, M. Brooks, P. G. Zotev, A. Genco, J. Cambiasso, S. Mignuzzi, S. A. Maier, G. Burkard, R. Sapienza, and A. I. Tartakovskii, Dielectric nanoantennas for strain engineering in atomically thin two-dimensional semiconductors, *ACS Photonics* **7**, 2413 (2020).
- [49] S. Kansara, S. K. Gupta, and Y. Sonvane, Effect of strain engineering on 2d dichalcogenides transition metal: a dft study, *Computational Materials Science* **141**, 235 (2018).
- [50] J. Palepu, P. P. Anand, P. Parshi, V. Jain, A. Tiwari, S. Bhattacharya, S. Chakraborty, and S. Kanungo, Comparative analysis of strain engineering on the electronic properties of homogenous and heterostructure bilayers of mox_2 ($x = \text{s, se, te}$), *Micro and Nanostructures* **168**, 207334 (2022).
- [51] W. Wu, J. Wang, P. Ercius, N. C. Wright, D. M. Leppert-Simenuer, R. A. Burke, M. Dubey, A. M. Dogare, and M. T. Pettes, Giant mechano-optoelectronic effect in an atomically thin semiconductor, *Nano letters* **18**, 2351 (2018).
- [52] M. Pandey, C. Pandey, R. Ahuja, and R. Kumar, Straining techniques for strain engineering of 2d materials towards flexible straintronic applications, *Nano Energy*, 108278 (2023).
- [53] A. Smiri, T. Amand, and S. Jaziri, Optical properties of excitons in two-dimensional transition metal dichalcogenide nanobubbles, *The Journal of Chemical Physics* **154** (2021).
- [54] J. Chaste, *Straintronique et transport thermique dans les matériaux 2D*, Ph.D. thesis, Université Paris Saclay (2023).
- [55] S. Ippolito, *Defect engineering in 2D semiconductors: fabrication of hybrid multifunctional devices*, Ph.D. thesis, Université de Strasbourg (2021).
- [56] M. Pandey and R. Kumar, Polymer curing assisted formation of optically visible sub-micron blisters of multilayer graphene for local strain engineering, *Journal of Physics: Condensed Matter* **34**, 245401 (2022).
- [57] S. Deng, L. Li, and Y. Zhang, Strain modulated electronic, mechanical, and optical properties of the monolayer pds_2 , pdse_2 , and ptse_2 for tunable devices, *ACS Applied Nano Materials* **1**, 1932 (2018).
- [58] O. Çakıroğlu, J. O. Island, Y. Xie, R. Frisenda, and A. Castellanos-Gomez, An automated system for strain engineering and straintronics of 2d materials, *Advanced Materials Technologies* **8**, 2201091 (2023).
- [59] F. Carrascoso, R. Frisenda, and A. Castellanos-Gomez, Biaxial versus uniaxial strain tuning of single-layer mos_2 , *Nano Materials Science* **4**, 44 (2022).
- [60] H. Ren and G. Xiang, Strain-modulated magnetism in mos_2 , *Nanomaterials* **12**, 1929 (2022).
- [61] Q.-L. Lin, Z.-F. Qian, X.-Y. Dai, Y.-L. Sun, and R.-H. Wang, Regulation of electronic structure of monolayer mos_2 by pressure, *Rare Metals* **41**, 1761 (2022).
- [62] C. Wang, S. Li, S. Wang, P. Zhao, and R. Zhuo, First principles study of the effect of uniaxial strain on monolayer mos_2 , *Physica E: Low-dimensional Systems and Nanostructures* **144**, 115401 (2022).
- [63] O. K. Le, V. Chihai, M.-P. Pham-Ho, *et al.*, Electronic and optical properties of monolayer mos_2 under the influence of polyethyleneimine adsorption and pressure, *RSC advances* **10**, 4201 (2020).
- [64] Y. Chen, D. Lu, L. Kong, Q. Tao, L. Ma, L. Liu, Z. Lu, Z. Li, R. Wu, X. Duan, *et al.*, Mobility enhancement of strained mos_2 transistor on flat substrate, *ACS nano* **17**, 14954 (2023).
- [65] L. Yang, X. Cui, J. Zhang, K. Wang, M. Shen, S. Zeng, S. A. Dayeh, L. Feng, and B. Xiang, Lattice strain effects on the optical properties of mos_2 nanosheets, *Scientific reports* **4**, 5649 (2014).
- [66] S.-D. Guo, Biaxial strain tuned thermoelectric properties in monolayer ptse_2 , *Journal of Materials Chemistry C* **4**, 9366 (2016).
- [67] X. Ge, X. Zhou, D. Sun, and X. Chen, First-principles study of structural and electronic properties of monolayer ptx_2 and janus ptxy ($x, y = \text{s, se, and te}$) via strain engineering, *ACS omega* **8**, 5715 (2023).
- [68] Z. Wang, X. Jing, S. Duan, C. Liu, D. Kang, X. Xu, J. Chen, Y. Xia, B. Chang, C. Zhao, *et al.*, 2d ptse_2 enabled wireless wearable gas monitoring circuits with distinctive strain-enhanced performance, *ACS nano* (2023).
- [69] P. Li, L. Li, and X. C. Zeng, Tuning the electronic properties of monolayer and bilayer ptse_2 via strain engineering, *Journal of Materials Chemistry C* **4**, 3106 (2016).
- [70] W. Zhang, J. Qin, Z. Huang, and W. Zhang, The mechanism of layer number and strain dependent bandgap of 2d crystal ptse_2 , *Journal of Applied Physics* **122** (2017).
- [71] Y. Han, L. Gao, J. Zhou, Y. Hou, Y. Jia, K. Cao, K. Duan, and Y. Lu, Deep elastic strain engineering of 2d materials and their twisted bilayers, *ACS Applied Materials & Interfaces* **14**, 8655 (2022).
- [72] Z. Hong, Tunable structure and electronic properties of multilayer ptse_2 , in *Journal of Physics: Conference Series*, Vol. 1411 (IOP Publishing, 2019) p. 012019.
- [73] H. J. Conley, B. Wang, J. I. Ziegler, R. F. Haglund Jr, S. T. Pantelides, and K. I. Bolotin, Bandgap engineering of strained monolayer and bilayer mos_2 , *Nano letters* **13**, 3626 (2013).
- [74] A. Armstrong, K. P. McKenna, and Y. Wang, Directional dependence of band gap modulation via uniaxial strain in mos_2 and tis_3 , *Nanotechnology* **35**, 015704 (2023).
- [75] A. E. Maniadaki, G. Kopidakis, and I. N. Remediakis, Strain engineering of electronic properties of transition metal dichalcogenide monolayers, *Solid State Communications* **227**, 33 (2016).

- [76] M. Sharma and R. Singh, Tuning electronic properties of pentagonal ptse_2 monolayer by applying external strain, *Indian Journal of Physics* **96**, 1037 (2022).
- [77] T.-Y. Su, T.-H. Wang, D. P. Wong, Y.-C. Wang, A. Huang, Y.-C. Sheng, S.-Y. Tang, T.-C. Chou, T.-L. Chou, H.-T. Jeng, *et al.*, Thermally strain-induced band gap opening on platinum diselenide-layered films: A promising two-dimensional material with excellent thermoelectric performance, *Chemistry of Materials* **33**, 3490 (2021).
- [78] P. Giannozzi, S. Baroni, N. Bonini, M. Calandra, R. Car, C. Cavazzoni, D. Ceresoli, G. L. Chiarotti, M. Cococcioni, I. Dabo, *et al.*, Quantum espresso: a modular and open-source software project for quantum simulations of materials, *Journal of physics: Condensed matter* **21**, 395502 (2009).
- [79] P. E. Blöchl, Projector augmented-wave method, *Physical review B* **50**, 17953 (1994).
- [80] R. P. Feynman, Forces in molecules, *Physical review* **56**, 340 (1939).
- [81] K. Momma and F. Izumi, Vesta 3 for three-dimensional visualization of crystal, volumetric and morphology data, *Journal of applied crystallography* **44**, 1272 (2011).
- [82] J. P. Perdew, K. Burke, and M. Ernzerhof, Generalized gradient approximation made simple, *Physical review letters* **77**, 3865 (1996).
- [83] P. Giannozzi, O. Andreussi, T. Brumme, O. Bunau, M. B. Nardelli, M. Calandra, R. Car, C. Cavazzoni, D. Ceresoli, M. Cococcioni, *et al.*, Advanced capabilities for materials modelling with quantum espresso, *Journal of physics: Condensed matter* **29**, 465901 (2017).
- [84] L. Fang, W. Liang, Q. Feng, and S.-N. Luo, Structural engineering of bilayer ptse_2 thin films: a first-principles study, *Journal of Physics: Condensed Matter* **31**, 455001 (2019).
- [85] M. S. Shawkat, J. Gil, S. S. Han, T.-J. Ko, M. Wang, D. Dev, J. Kwon, G.-H. Lee, K. H. Oh, H.-S. Chung, *et al.*, Thickness-independent semiconducting-to-metallic conversion in wafer-scale two-dimensional ptse_2 layers by plasma-driven chalcogen defect engineering, *ACS applied materials & interfaces* **12**, 14341 (2020).
- [86] R. A. B. Villaos, C. P. Crisostomo, Z.-Q. Huang, S.-M. Huang, A. A. B. Padama, M. A. Albao, H. Lin, and F.-C. Chuang, Thickness dependent electronic properties of pt dichalcogenides, *npj 2D Materials and Applications* **3**, 2 (2019).
- [87] K. Zhang, M. Yan, H. Zhang, H. Huang, M. Arita, Z. Sun, W. Duan, Y. Wu, and S. Zhou, Experimental evidence for type-ii dirac semimetal in ptse_2 , *Physical Review B* **96**, 125102 (2017).
- [88] F. Gronvold, H. Haraldsen, and A. Kjekshus, On the sulfides, selenides and tellurides of platinum, *Acta Chem. Scand* **14**, 1879 (1960).
- [89] T. Bucko, J. Hafner, S. Lebègue, and J. G. Ángyán, Improved description of the structure of molecular and layered crystals: ab initio dft calculations with van der waals corrections, *The Journal of Physical Chemistry A* **114**, 11814 (2010).
- [90] I. Hamada and M. Otani, Comparative van der waals density-functional study of graphene on metal surfaces, *Physical Review B* **82**, 153412 (2010).
- [91] K. Berland, Ø. Borck, and P. Hyldgaard, van der waals density functional calculations of binding in molecular crystals, *Computer Physics Communications* **182**, 1800 (2011).
- [92] H. Liu, P. Lazzaroni, and C. Di Valentin, Nature of excitons in bidimensional wse_2 by hybrid density functional theory calculations, *Nanomaterials* **8**, 481 (2018).
- [93] J. Chang, L. F. Register, and S. K. Banerjee, Ballistic performance comparison of monolayer transition metal dichalcogenide mx_2 ($m = \text{mo}, \text{w}$; $x = \text{s}, \text{se}, \text{te}$) metal-oxide-semiconductor field effect transistors, *Journal of Applied Physics* **115** (2014).
- [94] A. F. Allah, *Regroupement de techniques de caractérisation de matériaux destinés à l'énergie solaire pour optimisation et mesures industrielles*, Ph.D. thesis, Université Paris Sud-Paris XI (2015).
- [95] A. D. Yoffe, Low-dimensional systems: quantum size effects and electronic properties of semiconductor microcrystallites (zero-dimensional systems) and some quasi-two-dimensional systems, *Advances in Physics* **42**, 173 (1993).
- [96] H. L. Zhuang and R. G. Hennig, Computational search for single-layer transition-metal dichalcogenide photocatalysts, *The Journal of Physical Chemistry C* **117**, 20440 (2013).
- [97] L. Kou, B. Yan, F. Hu, S.-C. Wu, T. O. Wehling, C. Felser, C. Chen, and T. Frauenheim, Graphene-based topological insulator with an intrinsic bulk band gap above room temperature, *Nano letters* **13**, 6251 (2013).
- [98] L. Kou, S.-C. Wu, C. Felser, T. Frauenheim, C. Chen, and B. Yan, Robust 2d topological insulators in van der waals heterostructures, *ACS nano* **8**, 10448 (2014).